Global Coupling in the Presence of Defects: Synchronization in an Oscillatory Surface Reaction

G. Veser, F. Mertens, A. S. Mikhailov, and R. Imbihl
Fritz-Haber-Institut der Max-Planck-Gesellschaft, Faradayweg 4-6, D-14195 Berlin (Dahlem), Germany
(Received 8 March 1993)

The transition from a spatially uniformly oscillating surface to the formation of chemical wave patterns has been investigated in the NO+CO reaction on Pt(100) using photoemission electron microscopy. This transition is associated with a discontinuous jump in the local oscillation frequency and can be described as a breakdown of global coupling caused by the presence of defects in the oscillating medium.

PACS numbers: 82.65.Jv, 05.70.Ln

Reaction-diffusion systems are known to exhibit a large variety of different wave pattern solutions, which have been extensively studied both experimentally and theoretically [1,2]. For oscillatory media, it has been shown that the introduction of long range synchronization through a global coupling mode may lead to new phenomena such as standing waves which exist in a narrow parameter range and are caused by parametric resonance [3,4]. Otherwise, for a homogeneous medium, one obtains the seemingly trivial case of spatially uniform oscillations. In any realistic system, however, the properties of the medium will not be spatially uniform, but defects will be present. Evidently, defects will make synchronization more difficult and because synchronization is of fundamental importance in many physical, chemical, and biological systems, there is a clear need to investigate the competition between global coupling and defects [2].

Presented in the following is an experiment that demonstrates the scenario which develops in a medium with global coupling as the influence of defects is continuously increased. This causes a breakdown of global coupling, leading from spatially uniform oscillations to the formation of wave patterns, as the defects gain control over the oscillatory medium. One observes a discontinuous transition characterized by a collapse of the integral oscillation amplitude and by a jump in the frequency of the local oscillators. These experimental results are complemented by simulations with the complex Ginzburg-Landau equation, modified appropriately to take into account the effect of global coupling.

The experimental system we investigate is the catalytic reduction of NO with CO which proceeds according to the overall reaction $CO+NO \rightarrow CO_2+\frac{1}{2}N_2$ and which exhibits kinetic oscillations on a Pt(100) surface under isothermal low pressure conditions ($p \sim 10^{-6}$ Torr) [5–7]. Previous investigations have already shown that the diffusional coupling via the surface diffusion of adsorbed CO and NO leads to spatiotemporal pattern formation on the Pt(100) surface [7]. Aside from diffusional coupling, global coupling is also present, since, due to mass balance in the reaction, the variations in the reaction rate are accompanied by corresponding changes in the partial pressures of the reactants, CO and NO. These variations are typically on the order of $\approx 1\%$ of p_{CO} and p_{NO}. The global coupling mode is inefficient at low temperature but becomes essential for the oscillations at higher temperature ($T > 470$ K), a regime that will be examined more closely in the following.

The experiments are conducted in a standard UHV system which under reaction conditions (10^{-6} Torr) was operated as a gradient free flow reactor [6,7]. Spatially resolved measurements were conducted with the recently developed photoemission electron microscopy (PEEM) [8]. This method allows one to image the locally varying adsorbate concentration under reaction conditions, typically achieving a lateral resolution of ≈ 1 μm. The Pt(100) sample is $5\times5\times1$ mm^3 and is the same crystal as used in previous investigations [6,7].

The clean Pt(100) surface exhibits a quasihexagonal reconstruction ("hex"). This reconstruction, however, can be lifted upon CO or NO adsorption [6,9]. This constitutes an adsorbate induced $1\times1 \rightleftarrows$ hex surface phase transition (SPT) which is controlled by critical adsorbate coverages. As one adjusts p,T conditions such that the adsorbate coverage is just on the borderline of lifting the hex reconstruction ($\theta_{CO,crit} \approx 0.08$ [9]), one obtains kinetic oscillations which proceed on a largely hex reconstructed surface and which are coupled to periodic structural changes via the $1\times1 \rightleftarrows$ hex SPT [6]. In contrast to former investigations of this system [5,6], in which only damped oscillations are observed, we are able to obtain sustained oscillations in a very reproducible way by going through an extensive preparation procedure of the surface prior to each experiment [10].

Figure 1(a) depicts schematically the development of rate oscillations and of spatiotemporal patterns observed as one traverses the temperature window for the rate oscillations described above in the direction of decreasing T. Starting from a stationary reaction rate, first chaotic small amplitude oscillations develop. These chaotic oscillations are then transformed into stable period-1 oscillations by going in inverse direction through Feigenbaum cascade in which oscillations up to period 8 could be identified. During this entire sequence, the amplitude of the oscillations grows continuously while the surface displays spatially uniform oscillations in PEEM, associat-

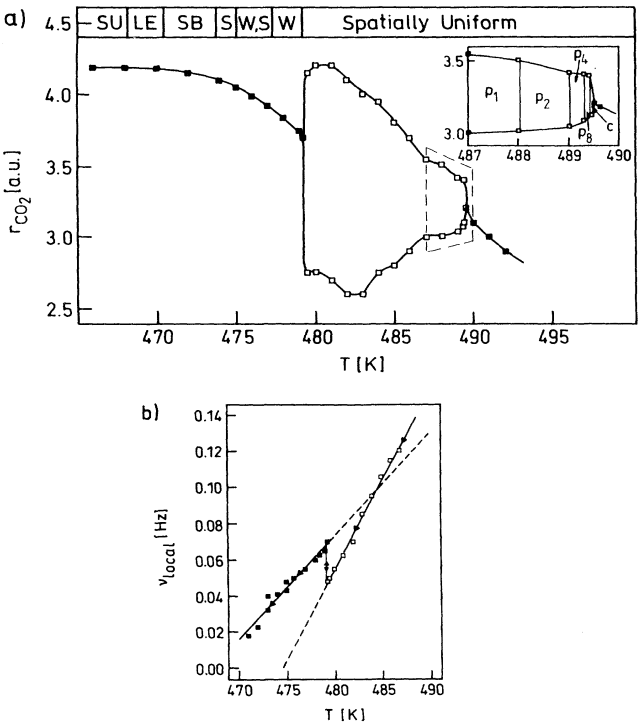

FIG. 1. Transition from spatially homogeneous rate oscillations to wave patterns in the NO+CO reaction on Pt(100). The experiments are conducted in the direction of decreasing temperature with $p_{NO}=4\times10^{-6}$ mbar and $p_{CO}=4\times10^{-6}$ mbar. (a) Bifurcation diagram showing the range where the CO_2 production r_{CO_2} is stationary (filled squares) and where the reaction rate exhibits kinetic oscillations. The oscillation amplitudes, i.e., the upper and lower turning points, are marked by open squares. The inset shows the Feigenbaum scenario which is found at the upper temperature boundary of the oscillatory range. The different types of spatial patterns which can be observed in PEEM are indicated schematically: SU=spatially uniform; W=wave trains; W,S=wave trains and spirals; S=spirals; SB=spiral breakup; LO=local outbursts. (b) Variation of the local oscillation frequency ν_{local} in the bifurcation scenario depicted in (a). The local oscillation frequency has been determined by integrating the intensity in a small spot of 20×20 μm^2 size in the PEEM images.

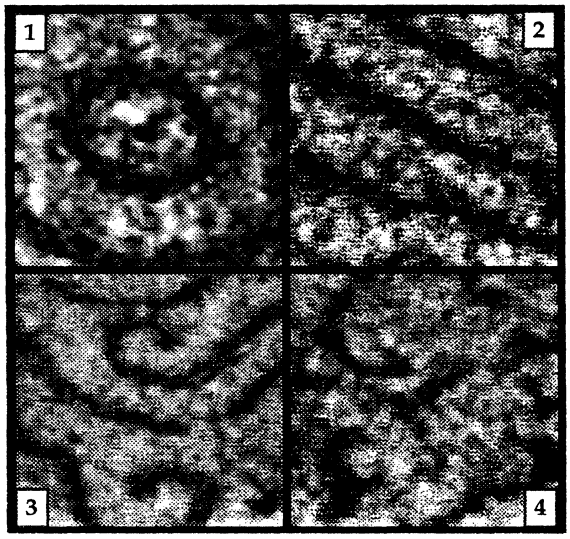

FIG. 2. Sequence of PEEM images demonstrating various stages of spatial pattern formation after the breakdown of global coupling, as is indicated in Fig. 1(a). (1) Defect emitting waves, $T=478$ K, (2) parallel wave trains, $T=477.5$ K, (3) formation of spiral waves, $T=475.5$ K, (4) local outbursts of activity, $T=472$ K. The size of the frames is 300×300 μm^2.

ed with only small intensity changes.

At $T=482$ K, the amplitude of the rate oscillations reaches a maximum and—after a decrease of $\approx10\%$—the amplitude collapses in a discontinuous transition at $T_{tr}=479.5$ K. At the same instant, periodic wave trains with a spatial periodicity of ≈70 μm and a velocity of ≈10 μm/s are visible in PEEM. By looking at the local oscillation frequency ν_{local} which is obtained by integrating the intensity in a small spot of the PEEM images and which is displayed in Fig. 1(b), one notes that the collapse of the rate oscillations causes ν_{local} to increase by nearly a factor of 2. The transition from the uniformly oscillating surface to the wave pattern has been investigated extensively and, within the experimental accuracy of ≈0.25 K, this transition always occurred discontinuously. Furthermore, no hysteresis effects were detectable in connection with the discontinuous transition (for $|T-T_{tr}|<1$ K).

As the temperature is lowered further, the plane wave fronts become unstable. Upon collision with inactive defects, they break up and the free ends curl up into pairs of spirals. At even lower temperature only spiral fragments can develop. Finally, after going through a range in which local outbursts of activity can still be observed, a spatially uniform stable state of the surface results. This scenario is illustrated by the PEEM images displayed in Fig. 2. The change from the appearance of a periodic wave pattern to the homogeneous state can be understood in a straightforward way as the transition from an oscillatory to an excitable medium followed by a continuous decrease in excitability.

The transition from the rate oscillations to the wave pattern reflects the breakdown of gas-phase coupling and, as will be demonstrated in the following, defects play an essential role in this process. In our case, these defects are structural imperfections on the surface of typically 1–5 μm diameter (density $\approx2/mm^2$) which are identifiable in PEEM (see Fig. 2, frame 1) and act as trigger centers for the wave trains. They differ from the defect free surface area ("bulk") in their oscillatory behavior, as one can see in Fig. 1(b). There the two kinds of oscillators give rise to two different slopes with the steeper one being associated with the bulk oscillations and the less

steep one belonging to the defects.

The same diagram also offers a qualitative explanation for the breakdown of gas-phase coupling. With decreasing temperature the difference in frequency between defects and the bulk becomes so large that gas-phase coupling is no longer strong enough to enforce complete synchronization, and some defects start to emit waves. Since the spatial average over a region filled with periodic waves is constant in time, global coupling vanishes. The abruptness of the transition can be explained with the positive feedback between the spreading of waves and the vanishing of global coupling.

To support the qualitative explanation of the observed effect of global coupling breakdown, we have performed a theoretical analysis with a simple mathematical model. As a basis for our model we used the complex Ginzburg-Landau (CGL) equation because this equation exhibits universal validity in the vicinity of a Hopf bifurcation and is known to characterize the principle properties of pattern formation in oscillatory media [11]. In order to account for the effect of gas-phase coupling, the CGL equation was modified by introducing an additional term. The model thus obtained describes a set of small-amplitude limit-cycle oscillators with local diffusional coupling between the neighbors and an additional global coupling. The complex local oscillation amplitude $\eta(x,t)$ obeys the equation

$$\dot{\eta}=[1-i\alpha-i\delta\omega(x)]\eta-(1-i\beta)|\eta|^2\eta + (1-i\varepsilon)\nabla^2\eta-\mu e^{i\chi}\bar{\eta}. \quad (1)$$

The last term in this equation, proportional to the spatial average $\bar{\eta}$ of local amplitudes η, takes into account global coupling. It represents a uniform driving force generated within the system and vanishing when the local oscillations become asynchronous; the parameter χ characterizes a phase shift between the acting force and the spatial average $\bar{\eta}$. The frequency of the individual oscillators described by Eq. (1) is $\omega=\alpha-\beta$. The defect is modeled assuming that inside the defect the oscillation frequency ω is increased by an amount $\delta\omega(x)$. In the numerical simulations we take $\delta\omega(x)=\delta\omega$ for $0\le x\le d$ and $\delta\omega(x)=0$ for $x>d$. We consider the case when $\varepsilon>\beta>0$ and $\mu\ll 1$.

If the wave patterns remain sufficiently smooth and are characterized by large enough wavelengths ($\lambda\gg 1$), they can be described using the phase equation [2,12]. Writing $\eta=\rho\exp[-i(\Omega t+\phi)]$ and $\bar{\eta}=R\exp[-i(\Omega t+\Psi)]$ where Ω is the frequency of the bulk oscillations, one derives from Eq. (1) an approximate dynamic equation for the slowly varying phase ϕ,

$$\dot{\phi}=(1+\varepsilon\beta)\nabla^2\phi+(\varepsilon-\beta)(\nabla\phi)^2 + \mu_1[R\sin(\chi_1+\phi-\Psi)-\sin\chi_1]+\delta\omega(x), \quad (2)$$

where $\mu_1=\mu(1+\beta^2)^{1/2}$ and $\chi_1=\chi-\arctan\beta$. Simple analysis shows that the locked-in uniform state $\phi=\Psi$ is stable in respect to small local perturbations if the condition $\cos\chi_1<0$ is satisfied.

We find that global coupling suppresses the autonomous activity of weak defects: They oscillate at frequency Ω of the bulk oscillations. A defect begins autonomous oscillations when its strength $\delta\omega$ exceeds a threshold $\delta\omega_{\rm th}$. The threshold can be estimated as $\delta\omega_{\rm th}=\mu_1(1+\sin\chi_1)$ for defects with sufficiently large spatial sizes $d\gg 1$. Above the threshold this defect becomes a pacemaker, i.e., a periodic source of propagating waves. The density of defects is not an important quantity in this context because a single defect suffices to initiate the breakdown of global coupling if its frequency is above a certain threshold. When the entire surface is covered by waves, global coupling vanishes. After the collapse of global coupling the local oscillation frequency of the medium's elements is determined by the frequency of the strongest critical defect and is thus increased with respect to that of bulk oscillations in the presence of global coupling.

We performed numerical simulations of these effects for model (1) in the case of a one-dimensional medium. The results of these simulations are displayed in Fig. 3 showing the collapse of the integral signal $\bar{\eta}$ and the jump in the local oscillation frequency that occurs when a su-

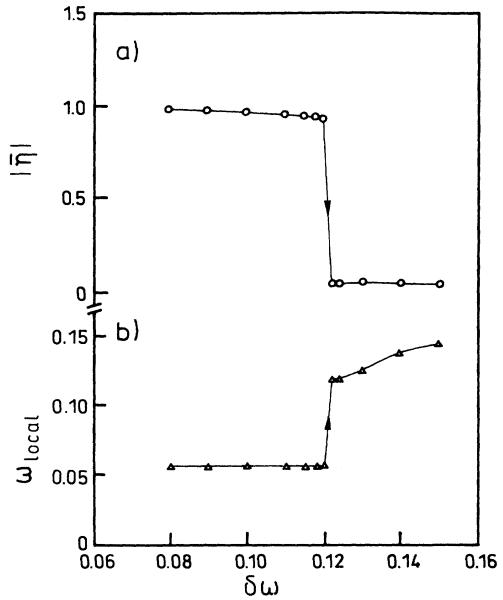

FIG. 3. Simulated breakdown of global coupling taking place as the frequency difference $\delta\omega$ between defect and bulk is increased beyond a threshold. The diagram displays the variation of the integral oscillation amplitude $\bar{\eta}$ (a) and of the local oscillation frequency $\omega_{\rm local}$ (b). The simulation results should be compared to a temperature range in the experimental data in Fig. 1, which extends from roughly 475 to 485 K. The model calculations were conducted with 1024 grid points using the following constants: $\alpha=0$, $\beta=1$, $\varepsilon=2$, $\mu=0.05$, $\chi=\pi$. The defect size was 64 grid points.

percritical defect gains control over the system. One notes that close to the transition point the integral signal $\bar{\eta}$ already begins to decrease slightly [see Fig. 3(a)]. This effect, which is also visible in the experimental curve in Fig. 1(a), can be attributed to the fact that near the transition point the oscillations inside the defect already exhibit a significant phase shift with respect to the bulk, although it is still not able to act as a pacemaker.

We note that the simulation yields the same scenario as is observed experimentally. The only qualitative difference is that a hysteresis is always observed in the numerical simulations, whereas it is absent in the experiment. From previous experiments, however, we know that the NO+CO reaction is extremely temperature sensitive and therefore a temperature change which is inherent in the experimental procedure will have an additional synchronizing effect on the local oscillators, which is not accounted for in the model [6].

When other assumptions about its parameters are made, the same model can demonstrate a variety of phenomena. If the conditions $\cos\chi_1 > 0$ and $1+\varepsilon\beta > 0$ are fulfilled, a spontaneous collapse of global coupling accompanied by formation of large spatial domains is observed. The effects of pattern formation described by a variant of Eq. (1) with external periodic forcing and $1+\varepsilon\beta < 0$ were recently discussed in [13]. Similar effects of spatial pattern formation may represent a transient stage for model (1) when condition $1+\varepsilon\beta < 0$ is satisfied. This transient would lead to a collapse of global coupling and carry the system directly into a turbulent regime. A possible experimental realization of this type of scenario may exist in another oscillatory surface reaction, namely the NO $+NH_3$ reaction on Pt(100) [14].

In summary, we have demonstrated that defects play an essential role in desynchronization since they can act as nuclei for the breakdown of global coupling. The presented scenario is apparently robust. Similar transitions can hence be expected in a wide variety of oscillatory systems.

The authors would like to thank S. Wasle for the preparation of the drawings. One of us (G.V.) is indebted to the Stiftung *Stipendienfonds des VCI* for financial support.

[1] See, e.g., the *Proceedings of the* NATO *Advanced Research Workshop on Non-Equilibrium Chemical Dynamics. From Experiment to Microscopic Simulations, Bruxelles, 1991* [Physica (Amsterdam) **188A**, Nos. 1-3 (1992)].
[2] Y. Kuramoto, *Chemical Oscillations, Waves and Turbulence* (Springer, Berlin, 1984).
[3] S. Jakubith, H. H. Rotermund, W. Engel, A. von Oertzen, and G. Ertl, Phys. Rev. Lett. **65**, 3013 (1990).
[4] H. Levine and X. Zou, Phys. Rev. Lett. **69**, 204 (1992).
[5] S. B. Schwartz and L. D. Schmidt, Surf. Sci. **206**, 169 (1988).
[6] T. Fink, J.-P. Dath, R. Imbihl, and G. Ertl, J. Chem. Phys. **95**, 2109 (1991).
[7] G. Veser and R. Imbihl, J. Chem. Phys. **96**, 7155 (1992).
[8] W. Engel, M. E. Kordesch, H. H. Rotermund, S. Kubala, and A. von Oertzen, Ultramicroscopy **36**, 148 (1991).
[9] R. J. Behm, P. A. Thiel, P. R. Norton, and G. Ertl, J. Chem. Phys. **78**, 7437 (1983); **78**, 7448 (1983).
[10] G. Veser and R. Imbihl (to be published).
[11] A. C. Newell, Lect. Appl. Math **15**, 157 (1974).
[12] P. Ortoleva and J. Ross, J. Chem. Phys. **58**, 5673 (1973).
[13] P. Coullet and K. Emilsson, Physica (Amsterdam) **188A**, 190 (1992).
[14] G. Veser, F. Esch, and R. Imbihl, Catal. Lett. **13**, 371 (1992).

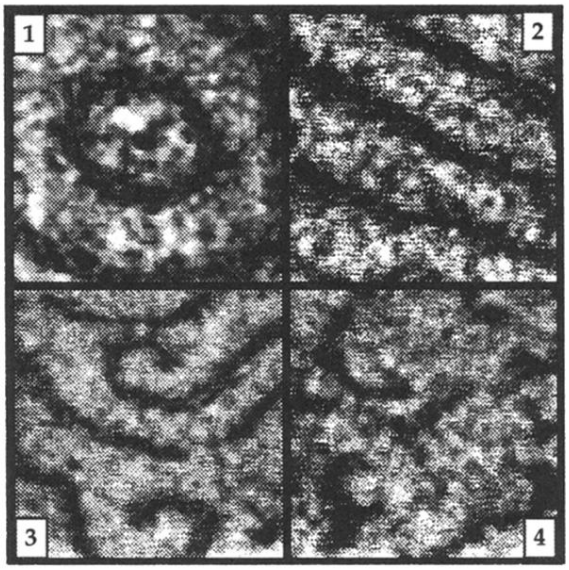

FIG. 2. Sequence of PEEM images demonstrating various stages of spatial pattern formation after the breakdown of global coupling, as is indicated in Fig. 1(a). (1) Defect emitting waves, $T=478$ K, (2) parallel wave trains, $T=477.5$ K, (3) formation of spiral waves, $T=475.5$ K, (4) local outbursts of activity, $T=472$ K. The size of the frames is 300×300 μm^2.